Interaction of the Disaccharide Trehalose with a Phospholipid Bilayer: A Molecular Dynamics Study

Cristina S. Pereira,*† Roberto D. Lins,* Indira Chandrasekhar,* Luiz Carlos G. Freitas,† and Philippe H. Hünenberger*

*Laboratory of Physical Chemistry, Eidgenössische Technische Hochschule, Hönggerberg, HCI, CH-8093 Zürich, Switzerland; and †Departamento de Química, Universidade Federal de São Carlos, 13565905 São Carlos, SP, Brazil

ABSTRACT The disaccharide trehalose is well known for its bioprotective properties. Produced in large amounts during stress periods in the life of organisms able to survive potentially damaging conditions, trehalose plays its protective role by stabilizing biostructures such as proteins and lipid membranes. In this study, molecular dynamics simulations are used to investigate the interaction of trehalose with a phospholipid bilayer at atomistic resolution. Simulations of the bilayer in the absence and in the presence of trehalose at two different concentrations (1 or 2 molal) are carried out at 325 K and 475 K. The results show that trehalose is able to minimize the disruptive effect of the elevated temperature and stabilize the bilayer structure. At both temperature, trehalose is found to interact directly with the bilayer through hydrogen bonds. However, the water molecules at the bilayer surface are not completely replaced. At high temperature, the protective effect of trehalose is correlated with a significant increase in the number of trehalose-bilayer hydrogen bonds, predominantly through an increase in the number of trehalose molecules bridging three or more lipid molecules.

INTRODUCTION

Nature has developed numerous strategies for the long-term survival of organisms. Among the most intriguing are the biological mechanisms that preserve living organisms exposed to damaging conditions like extreme cold, dryness, or heat, or the absence of oxygen (Feofilova, 2003). This phenomenon, named cryptobiosis, involves a reversible suspension of the metabolism and an effective isolation from the environmental changes (Keilin, 1959; Clegg, 2001). Cryptobiosis is widespread in the animal and plant kingdoms, and occurs for example in tardigrades, nematodes, cysts of crustaceans, yeasts, bacteria, fungi, mosses, pollens, seeds, and even in entire higher plants (Clegg, 2001; Crowe et al., 1992; Guppy and Withers, 1999; Feofilova, 2003). A common feature of cryptobiotic processes is the production of large amounts of saccharides triggered by the detection of stressful conditions (Crowe et al., 2002; Crowe, 2002). However, the mechanisms whereby sugars may stabilize living systems during freeze-thaw, heat-cooling, or dehydration-rehydration cycles remain a matter of debate.

In the specific case of anhydrobiosis, three main hypotheses have been put forward to explain the protective effect of sugars. The water-replacement hypothesis suggests that during drying, sugars can substitute water molecules (in particular by forming hydrogen bonds) around the polar and charged groups present in phospholipid membranes and proteins, thereby stabilizing their native structure in the absence of water (Crowe et al., 1984, 1992, 1997, 1998b; Carpenter et al., 1994). The water entrapment hypothesis, in contrast, proposes that sugars concentrate residual water molecules close to the biostructure, thereby preserving to a large extent its solvation and native properties (Belton and Gil, 1994; Cottone et al., 2002; Lins et al., 2003). This hypothesis has been formulated in the context of proteins, based on thermodynamic data in solution showing that sugars are excluded from the biomolecular surface by water (Timasheff, 1982; Xie and Timasheff, 1997). Finally, the vitrification hypothesis suggests that sugars found in anhydrobiotic systems, known to be good vitrifying agents, protect biostructures through the formation of amorphous glasses, thereby reducing structural fluctuations and preventing denaturation or mechanical disruption (Sun and Leopold, 1994, 1997; Sun et al., 1994, 1996; Williams and Leopold, 1989).

In the last few years, a consensus has emerged that these mechanisms are not necessarily mutually exclusive (Clegg, 2001; Crowe et al., 1998a, 2002; Crowe, 2002; Carpenter et al., 1994; Sun and Leopold, 1997). Vitrification may occur simultaneously with a direct interaction of the biostructure with the sugar, or with an entrapment of residual water at its surface, depending on the type of the protected biostructure and on the nature of the environmental stress imposed on the organism. Additionally, some experimental investigations have suggested that other solutes (e.g., polyfructoses, arbutin, abcissic acid, and several families of stress proteins) may play a critical role in the protection of cells, which in some cases could be interconnected with the action of the saccharides (Singer and Lindquist, 1998; Oliver et al., 2001; Clegg, 2001; Crowe et al., 2002).

Among the sugars related with the mechanisms of cryptobiosis, trehalose (TRH) is one of the most effective protectants and has therefore been extensively studied

Submitted October 27, 2003, and accepted for publication December 18, 2003.

Address reprint requests to Philippe H. Hünenberger, Laboratory of Physical Chemistry, ETH-Hönggerberg, HCI G233, CH 8093 Zürich, Switzerland. Tel.: +41-1-632-5503; Fax: +41-1-632-1039; E-mail: phil@igc.phys.chem.ethz.ch.

0006-3495/04/04/2273/13 $2.00

(Crowe et al., 2001; Richards et al., 2002; Elbein et al., 2003). TRH is a nonreducing disaccharide consisting of two glucopyranose units in α-(1→1) linkage. This naturally occurring compound is the principal carbohydrate component (~80–90%) in the hemolymph of insects (Wyatt and Kalf, 1957) and is also commonly found in yeasts and mushrooms (Birch, 1972; Koch and Koch, 1925).

Studies on the metabolism of tardigrades (Westh and Ramlov, 1991; Somme, 1996), nematodes (Madin and Crowe, 1975; Behm, 1997), yeasts (Singer and Lindquist, 1998; Damore et al., 1991; Eleutherio et al., 1993), resurrection plants (Scott, 2000; Wingler, 2002), and *Artemia* species (Clegg, 1965, 1997; Clegg and Jackson, 1992) have shown that these organisms accumulate TRH in large concentrations during anhydrobiosis, heat shock, or osmotic stress. Several studies have established that TRH stabilizes biostructures such as membranes and proteins under unfavorable conditions (Crowe et al., 1984, 1987, 2003; Nakagaki et al., 1992; Hoekstra et al., 1997). In numerous situations, TRH has been found superior to other common mono- and disaccharide in terms of its protecting ability (Crowe et al., 1987).

The high efficiency of TRH as a bioprotector has been the subject of interesting discussions (Crowe et al., 1987, 2001). Different possible reasons have been put forward to explain the superiority of TRH, including a high glass-transition temperature, a large hydration radius, or peculiarities in the phase diagram of TRH-water mixtures. Several experimental (Branca et al., 1999, 2003; Sussich et al., 2001; Ballone et al., 2000) and theoretical (Liu et al., 1997; Conrad and de Pablo, 1999; Engelsen and Perez, 2000) studies have investigated the properties of TRH in solution and in the solid state, attempting to provide a better understanding of the connection between these so-called anomalous properties and the outstanding bioprotective ability of TRH. However, a consensus opinion has not yet emerged.

The particular properties of TRH have given rise to a surprisingly wide range of applications of this disaccharide in technology including the stabilization of proteins, membranes, liposomes, and vaccines (Crowe et al., 2001), the hypothermic storage of mammalian cells and organs (Crowe et al., 2003; Fukuse et al., 1999; Eroglu et al., 2002), and its use in cosmetics (Norcia, 2000) and food products (Richards et al., 2002). TRH also appears to be efficient in the treatment of dry eye syndrome, for which it is currently being tested in human clinical trials (Matsuo, 2001; Matsuo et al., 2002).

It has been clearly evidenced experimentally that TRH is able to stabilize biomembranes and model lipid bilayers exposed to damaging conditions (Crowe et al., 1984, 1987, 2001). In particular, TRH is able to inhibit fusion between bilayers, leakage, lateral phase separations, and the formation of nonbilayer phases (Crowe et al., 1987, 2001; Hoekstra et al., 1997). It has been suggested that TRH reduces the mechanical stress imposed on the membrane upon dehydration (lipid chains brought into close contact) by maintaining the spacing between the headgroups and, consequently, keeping the membrane in the fluid phase. Direct interaction between lipid and TRH molecules through the formation of hydrogen bonds has been demonstrated by several experimental techniques including infrared spectroscopy, differential scanning calorimetry, nuclear magnetic resonance (NMR), and x-ray diffraction (Crowe et al., 1984; Lee et al., 1986; Nakagaki et al., 1992; Tsvetkova et al., 1998; Nagase et al., 1999; Luzardo et al., 2000; Lambruschini et al., 2000; Ricker et al., 2003). This indicates that TRH molecules are located close to the lipid headgroups, possibly mimicking the solvation by water molecules. Several authors attribute the stabilizing effect of TRH to this direct interaction with the membrane, i.e., in terms of the previously mentioned water-replacement hypothesis (Crowe et al., 1987, 1992, 1997, 1998b). Other authors, after the theory proposed by Bryant and Wolfe for the stabilization of membranes by solutes (Bryant and Wolfe, 1992; Wolfe and Bryant, 1999), attribute the stabilization by TRH to a purely mechanical effect. This corresponds to the vitrification hypothesis, involving the formation of a TRH glassy matrix that mechanically hinders phase changes and conformational fluctuations in the lipid bilayer (Koster et al., 1994, 2000; Zhang and Steponkus, 1996). This hypothesis is able to provide an explanation for the differences in protecting abilities among different vitrifying agents and for the higher efficiency of TRH as a stabilizer. The theory does not exclude the possibility of specific hydrogen bonds between lipid and sugar molecules. However, such interactions are not viewed as a determinant factor in the stabilization process (Koster et al., 2000; Wolfe and Bryant, 1999).

In the last decades, numerous experimental studies have addressed the problem of TRH-membrane interactions. However, only two theoretical investigations relying on modeling methods (energy minimization protocols) have been reported (Chandrasekhar and Gaber, 1988; Rudolph et al., 1990). These two investigations showed that, in the absence of water, TRH is able to form energetically stable conformations bridging a number of lipid molecules (Chandrasekhar and Gaber, 1988). However, an extension of the method to sucrose and glucose did not succeed in reproducing the experimental order for the stabilizing efficiency of these sugars (Rudolph et al., 1990). Although TRH-protein interactions have been studied by atomistic simulations (Cottone et al., 2001, 2002; Lins et al., 2003), no simulations of TRH-membrane systems have been reported to date. Therefore a detailed picture for the molecular mechanism responsible for membrane stabilization is still lacking.

In this work, molecular dynamics (MD) simulations are used to investigate TRH-membrane interactions in moderately concentrated TRH solutions at the atomistic level. A bilayer of dipalmitoylphosphatidylcholine (DPPC) in the liquid-crystalline phase is used as a membrane model.

Simulations of the bilayer in the presence and in the absence of TRH are performed at two different temperatures, in an attempt to better understand the mechanisms of action of the disaccharide under extreme conditions.

METHODS

Molecular dynamics simulations

All MD simulations were performed using the GROMOS96 program (van Gunsteren et al., 1996) together with extensions of the GROMOS96 45A3 force field (Schuler et al., 2001) developed for lipids (Chandrasekhar et al., 2003) and carbohydrates (R. D. Lins and P. H. Hünenberger, unpublished results), and the simple point charge (SPC) water model (Berendsen et al., 1981). Newton's equations of motion were integrated based on the leapfrog algorithm (Hockney, 1970) using a 2-fs time step. The SHAKE method (Ryckaert et al., 1977) was applied to constrain all bonds lengths with a relative geometric tolerance of 10^{-4}. The simulations were carried out in the isothermal-isobaric (NPT) ensemble. The temperature was maintained by coupling separately the solute and solvent degrees of freedom to a heat bath (Berendsen et al., 1984) with a relaxation time of 0.1 ps. The pressure was maintained at 1 atm using coupling to a pressure bath via anisotropic coordinate scaling (Berendsen et al., 1984) with a relaxation time of 0.5 ps and an isothermal compressibility of 0.46×10^3 (kJ mol^{-1} nm^{-3})$^{-1}$. The nonbonded interactions were handled using a twin-range cutoff scheme (van Gunsteren and Berendsen, 1990). Within a short-range cutoff radius of 0.8 nm, the interactions were evaluated every time step based on a pair list recalculated every 5 steps. The intermediate-range interactions up to a long-range cutoff radius of 1.4 nm were evaluated simultaneously with each pair list update, and assumed constant in between. To account for electrostatic interactions beyond the long-range cutoff radius, a reaction-field approximation (Tironi et al., 1995) was applied using a relative dielectric permittivity of 54 for the solvent. For all simulations the atomic coordinates were saved every 1 ps for analysis.

Molecular systems

A hydrated membrane bilayer of 2×64 DPPC molecules was simulated in the presence of different TRH concentrations and at two different temperatures (325 K and 475 K). A total of six simulations were performed involving 1), the DPPC bilayer in pure water at 325 K or 475 K (control simulations); 2), the DPPC bilayer in a 1 molal (m) TRH solution (64 molecules) at 325 K or 475 K; and 3), the DPPC bilayer in a 2 m TRH solution (128 molecules) at 325 K or 475 K.

The highest temperature is not meant to represent a physical situation. It is used here as a mere device to place the bilayer under stress conditions and investigate how TRH affects the response of membrane.

The concentrations of the solutions in the systems with 64 and 128 TRH molecules are exactly 1.06 and 2.12 m respectively. For simplicity these concentrations will be referred as 1 m and 2 m. These correspond to ~21% and 42% solutions, respectively, in terms of w/w [TRH/(TRH + water)] units. The corresponding molarities (estimated at the beginning of the production runs at 325 K) are ~0.6 M and 1 M, respectively. However, the use of molalities (mol solute per kilogram solvent) is preferred here since these are independent of the volume of the system. The two concentrations considered here were selected within the range of values probed by different experimental studies of TRH-membrane systems in vitro (Nakagaki et al., 1992; Takahashi et al., 1997; Nagase et al., 1999; Luzardo et al., 2000). Note, however, that these concentrations are significantly lower than those consider in dehydration experiments (Crowe et al., 1998a).

A DPPC bilayer at full hydration (3655 molecules i.e., between 28 and 29 water molecules per lipid) in the liquid crystalline phase, previously equilibrated during a 2.5-ns MD simulation at 325 K, was used as the initial structure for all simulations. This configuration was taken without alterations for the production runs corresponding to the simulations without TRH. In the simulations including TRH, the water molecules were removed and 64 (1-m solution) or 128 (2-m solution) TRH molecules uniformly distributed in the system, maintaining a distance of at least 0.5 nm from each other and from the two surfaces of the bilayer. The systems were then resolvated using 3339 water molecules (between 26 and 27 water molecules per lipid), imposing a minimal distance of 0.28 nm between water molecules and any solute atom. The box dimensions in the x an y directions were approximately the same for all systems (5.8×6.2 nm) and increased in the z direction with increasing TRH concentration (7.3 nm, 7.8 nm, and 8.5 nm for 0 m, 1 m, and 2 m TRH, respectively) .

Equilibration

For the systems without TRH, the configuration equilibrated at 325 K during 2.5 ns was directly used to initiate two 6-ns production simulations, either at the same temperature or at an increased temperature of 475 K. For the systems including TRH, a thorough equilibration procedure was first performed to permit an adequate relaxation of the TRH molecules around the bilayer. The system (DPPC, TRH, and the newly introduced solvent molecules) was energy-minimized using 1000 steps of steepest descent, followed by a 1.5-ns preequilibration MD at 325 K and constant volume. At this point the temperature was raised to 500 K, and a 5-ns MD equilibration was performed at this temperature and at constant volume, with position constraints on all atoms of the bilayer. The distributions of specific DPPC, TRH, and water atoms along the bilayer normal (z axis) for the system containing TRH 2 m, corresponding to the beginning of the preequilibration at 325 K and to the end of the equilibration at 500 K, are shown in Fig. 1. The TRH molecules, which were initially distributed roughly in two layers (reminiscent of their arbitrary initial placement), acquire a more homogeneous distribution with an increased density close to the membrane surfaces during the equilibration. Similar observations were made for the system containing TRH 1 m (data not shown). The simulations at 325 K and 475 K were branched from the final configurations of the corresponding equilibration runs at 500 K. The

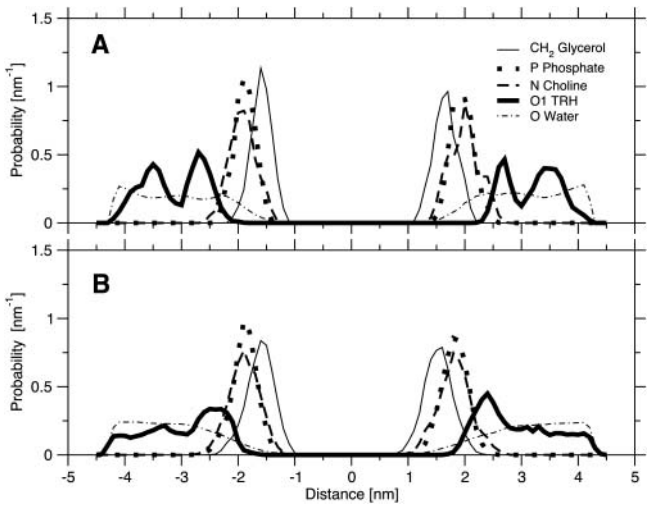

FIGURE 1 Normalized density profiles for specific atoms of DPPC, TRH, and water along the bilayer normal (z axis) for the system containing TRH 2 m at the beginning of the 325-K preequilibration run (A) and at the end of the 500-K equilibration run (B). The profiles correspond to averages over 0.25-ns periods.

systems were first relaxed by 250-ps MD at the corresponding temperature (maintaining the bilayer atoms fixed). For the system at 475 K this was followed by a further 100-ps MD period split into four blocks with gradually decreasing harmonic position restraint on the bilayer atoms. At this point, the four (two concentrations and two temperatures) 6-ns production simulations were started.

Analyses

The average area per lipid for the DPPC molecules was evaluated by dividing the surface of the *xy* plane of the simulation box by the number of lipids per layer (64).

The deuterium order parameters (S_{CD}) for the two acyl chains of DPPC (*sn*-1 and *sn*-2 chains) were evaluated in the simulations from the long-time average of the correlation function (second-order Legendre polynomial) describing the reorientation of the C-D vectors. More specifically, the order-parameter tensor for a carbon C_n along the chain is defined by $S_{ij} = 1/2\langle 3\cos\theta_i \cos\theta_j - 1\rangle$, where θ_i is the angle between the i^{th} molecular axis at C_n and the bilayer normal, which in the this case coincides with the *z* axis of the simulation box (Egberts and Berendsen, 1988). The molecular axes at a carbon C_n were defined according to the convention of Egberts and Berendsen (1988). The reported order parameter S_{CD} is the S_{zz} element of the tensor. The average was taken over time and over the 128 DPPC molecules.

Normalized density profiles were calculated for specific atoms of DPPC, TRH, and water along the bilayer normal (*z* axis of the simulation box). The atoms considered in this analysis were the phosphorus atom (phosphate group of DPPC), the nitrogen atom (choline group of DPPC), the united atom CH_1 (glycerol group of DPPC), the glycosidic oxygen (TRH), and the oxygen atom (water).

Diffusion coefficients (*D*) were calculated for DPPC, TRH, and water molecules. These were obtained from the Einstein relation $2NDt = \langle|R(t) - R(0)|^2\rangle$ (valid for long times *t*), where the right-hand side of the equation refers to the mean-square positional displacement of a specific atom, and *N* is the number of translational degrees of freedom considered. The atoms considered were the glycerol CH_1 united atom for DPPC, the glycosidic oxygen atom for TRH, and the oxygen atom for water. The average was taken over all DPPC, TRH, or water molecules, respectively. Due to the anisotropy of the system, the diffusion constants for TRH and water were calculated separately in the *xy* plane (D_{xy}, with $N = 2$) and along *z* axis (D_z, with $N = 1$). In the former case the time interval (*t*) considered was the overall time of the production runs. In the latter case, the motion of molecules along the *z* axis is restricted by the planes of the bilayer, and the time interval considered was that for which the mean-square positional displacement remains approximately linear as a function of time (typically 200 ps for the simulations at 325 K or 20 ps for the simulations at 475 K). The plateau value ΔR_z^2 of the mean-square displacement along the *z* axis is also reported in this case.

Hydrogen bonds (H-bonds) were monitored and classified according to the pairs of species present in the simulations (TRH–TRH, TRH–DPPC, TRH–water, and DPPC–water). The criterion used to define a H-bond was a hydrogen-acceptor distance shorter than 0.25 nm and a donor-hydrogen-acceptor angle larger than 135°. All the oxygen atoms of DPPC and TRH were considered as H-bond acceptors and all the hydroxyl groups of TRH as H-bond donors. The interaction between TRH and DPPC was further characterized by analyzing the patterns of H-bonding presented by the different TRH molecules. A pattern is noted by a series of integers (in descending order) indicating the number of H-bonds formed between a TRH molecule and DPPC molecules. For example, the pattern 211 represents a TRH molecule simultaneously doubly hydrogen bonded to a given DPPC molecule and singly hydrogen bonded to two other DPPC molecules. The results are presented as the number of TRH molecules belonging to a specified pattern of connectivity, averaged over the whole trajectory. The data are also presented in terms of the degree of bridging (number of distinct DPPC molecules forming at least one H-bond with a TRH molecule, e.g., three for the pattern 211).

RESULTS AND DISCUSSION

Simulations at 325 K

At 325 K the area per lipid for the DPPC bilayer in the presence of TRH (at either 1 m or 2 m) is slightly increased compared to the simulation without TRH (Fig. 2 *a*). The corresponding values of 0.56 nm^2 and 0.58 nm^2 (averaged over the last 1 ns of the simulations without and with TRH, respectively) are in the expected range for a fully hydrated DPPC membrane simulated using the current force field and simulations conditions (Chandrasekhar et al., 2003). This area per lipid is known to be on the low side compared to the best estimate of 0.64 nm^2 based on a careful analysis of the different available experimental values (Nagle and Tristram-Nagle, 2000). However, the difference may arise (at least in part) from the microscopic size and artificial periodicity of the simulated membrane patch that, unlike its experimental counterpart, cannot undergo undulations over a significant length scale. The slight expansion of the membrane in the presence of TRH agrees with experimental studies of DPPC (and other lipids) suggesting that TRH molecules intercalate between the lipid headgroups, thereby increasing the spacing between the lipid chains (Nakagaki et al., 1992; Luzardo et al., 2000; Takahashi et al., 1997). This observation should, however, be taken with some caution since the observed variation is of the same order of magnitude as the fluctuations in the area per lipid monitored during a longer simulation of the same DPPC membrane model in pure water (average area of 0.57 nm^2 with a standard deviation of 0.005 nm^2, data not shown). The time evolution of the box volume is essentially constant in the three simulations (Fig. 2 *b*), indicating that equilibrium has been reached for the average system density.

At 325 K, the ordering of the lipid chains is only weakly affected by the presence of TRH, as can be seen from the order parameters (S_{CD}) calculated for the consecutive atoms of the *sn*-1 and *sn*-2 chains of DPPC (Fig. 3, *a* and *b*). The order parameters slightly decrease upon inclusion of TRH 1 m. However, increasing the TRH concentration to 2 m does not appear to enhance this trend. Note that the S_{CD} values for the *sn*-2 chain in the absence of TRH are slightly overestimated compared to experimental data (Douliez et al., 1995), a known feature of the lipid force field employed in these simulations (Chandrasekhar et al., 2003).

The mobility of DPPC, TRH, and water molecules is also only moderately affected by changes in the TRH concentration, as can be seen from the lateral (D_{xy}) and transverse (D_z) diffusion coefficients calculated for these species (Tables 1 and 2). The diffusion coefficients of water systematically decrease upon increasing the TRH concentration, but at most by a factor two when the concentration is raised from 0 m to 2 m. On the other hand, the diffusion of TRH molecules is essentially unaffected upon doubling the TRH concentration. Note that the lateral diffusion constants for both water and TRH are systematically higher than the transverse ones,

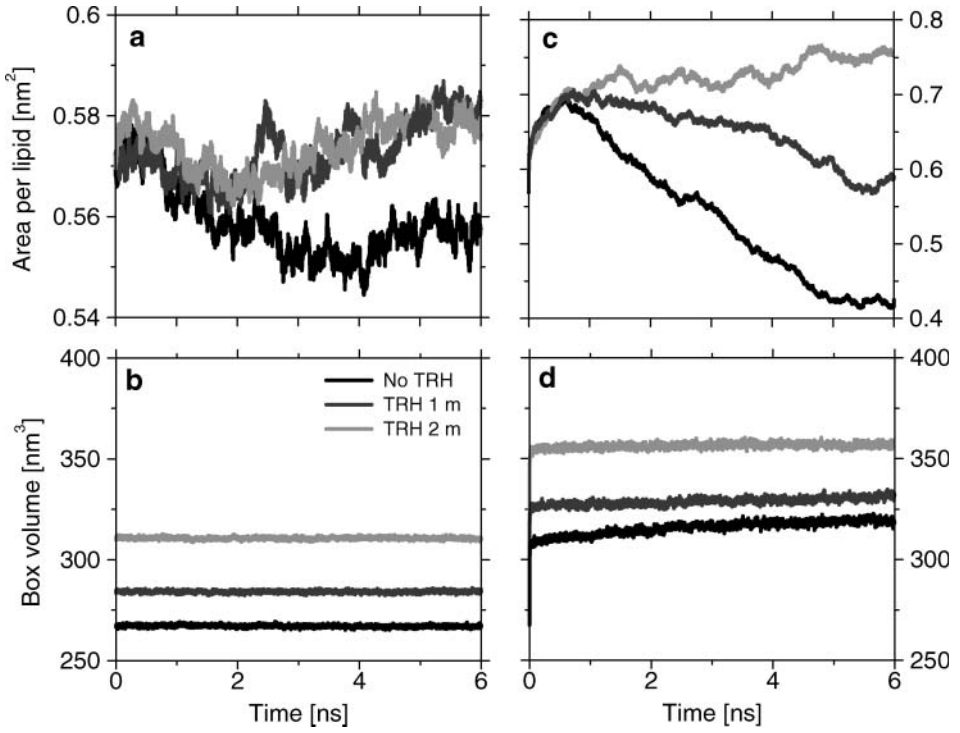

FIGURE 2 Area per lipid and box volume as a function of time, for the simulations with different TRH concentrations at 325 K (*a* and *b*) and 475 K (*c* and *d*). Note the different scales of graphics *a* and *c*.

a consequence of the restricted diffusion (bounded mean-square atomic displacements due to the impossibility of crossing the membrane plane) along the *z* axis (bilayer normal). The values of D_{xy} for water (2.41×10^{-5} cm^2/s) and TRH (1.49×10^{-6} cm^2/s) in the 2-m system are in good qualitative agreement with experimental results for the diffusion of water ($D = 1.05 \times 10^{-5}$ cm^2/s) and TRH ($D = 1.51 \times 10^{-6}$ cm^2/s) in a 44% TRH solution at 323 K (Ekdawi-Sever et al., 2003). In contrast to the other species, the lateral diffusion constant of the DPPC molecules

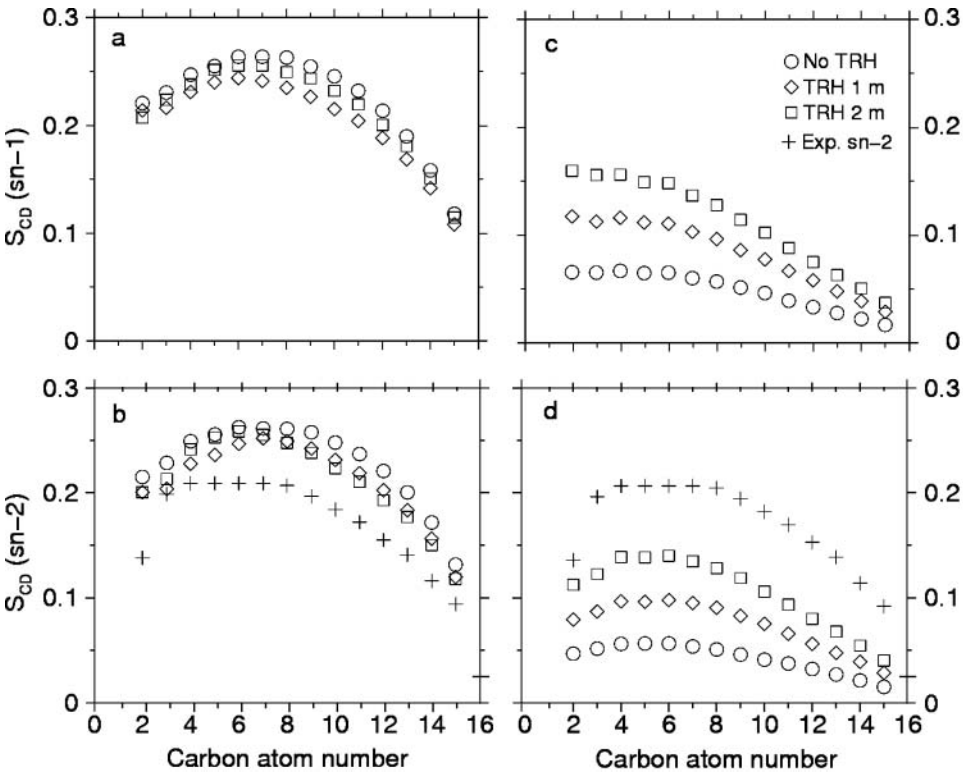

FIGURE 3 Deuterium order parameters (S_{CD}) as function of the carbon atom number along the *sn*-1 and *sn*-2 chains of DPPC calculated for the different simulations, i.e., at 325 K for the *sn*-1 (*a*) and *sn*-2 (*b*) chains and at 475 K for the *sn*-1 (*c*) and *sn*-2 (*d*) chains. Experimental values for the *sn*-2 chain at 325 K (Douliez et al., 1995) are given for comparison. The values are averaged over 128 DPPC molecules and over the 6-ns simulations.

TABLE 1 Lateral (D_{xy}) and transverse (D_z) diffusion coefficients for water molecules during the different simulations

C_{TRH} (m)	T (K)	D_{xy} (10^{-5} cm^2 s^{-1})	D_z (10^{-5} cm^2 s^{-1})	ΔR_z^2 (nm^2)
0	325	4.80	2.48	2.27
1	325	3.61	2.12	2.18
2	325	2.41	1.79	3.06
0	475	171	114	31.02
1	475	163	168	8.38
2	475	171	134	4.81

The plateau value (ΔR_z^2) of the mean-square displacement along the z axis is also reported.

increases approximately by a factor three upon increasing the TRH concentration from 0 m to 2 m. The values for the lateral diffusion of DPPC are of the same order of magnitude as those obtained from neutron scattering measurements ($D_{lat} = 1 \times 10^{-7}$ cm^2/s) (Sackmann, 1995). However, it should be stressed that the diffusion coefficients calculated for DPPC are only indicative, since the mean-square positional displacement is only approximately linear in time on the 6-ns timescale. The limited changes in the mobility of the three species indicate the system is still in a diffusive (as opposed to a glassy) state even at the highest TRH concentration.

The distributions of specific TRH, DPPC, and water atoms along the bilayer normal, averaged over the last 0.25 ns of the simulations (Fig. 4, *a–c*), show that the membrane remains intact in all cases. However, the distributions of the individual lipid atoms are somewhat broader in the presence of TRH. The density peaks observed for TRH in the vicinity of the bilayer surfaces (from five- to 10-fold increase compared to the bulk concentration), as well as the overlap between these density peaks and those corresponding to the DPPC headgroups, indicate that many TRH molecules interact tightly with the membrane. Note also that the TRH distribution is more homogeneous at 2 m compared to 1 m, suggesting that the membrane may have reached saturation between these two concentrations. Finally, it appears that water molecules are not excluded from the membrane surface upon coating by TRH molecules.

A direct evidence for the interaction between TRH and DPPC molecules is provided by the analysis of hydrogen bonds (H-bonds). The total number of H-bonds present on average between the different species in the system, together with this quantity scaled by the total number of interacting partners, are reported in Table 3. The latter quantity indicates the expected number of H-bonds between any two molecules of the corresponding species selected at random in the system (reported in percent). Among all species present, the highest H-bonding probability is found for pairs involving TRH and DPPC molecules. This result certainly indicates a high H-bonding affinity between these two types of molecules, but is also related to the fact that TRH and DPPC contain a large number of groups able to form H-bonds. As expected, doubling the TRH concentration increases the average number of TRH–DPPC, TRH–TRH, and TRH–water H-bonds. However, the TRH–DPPC H-bond probability actually decreases upon increasing the TRH concentration. This feature is indicative of saturation effects, as previously suggested by the analysis of Fig. 4, *b* and *c*. The number of H-bonds between DPPC and water decreases by 19% upon raising the TRH concentration from 0 m to 1 m. However, doubling the concentration of TRH does not significantly alter this number.

The observation that the sum of the TRH–DPPC and water–DPPC H-bonds at both TRH concentrations is almost equal to the number of water–DPPC H-bonds in the system without TRH agrees with the previous statement that water is not completely excluded from the membrane surface upon coating by TRH. Rather, TRH appears to replace water at about one-fifth of the H-bonding sites provided by the membrane surface.

Simulations at 475 K

At 475 K, the area per lipid for the DPPC bilayer is characterized by an initial expansion (~20% within 1 ns), followed by very different behaviors depending on the TRH concentration (Fig. 2 *c*). A large systematic decrease is observed during the simulation without TRH. The rate of decrease is somewhat smaller in the presence of TRH 1 m. In contrast, the simulation with TRH 2 m is characterized by an almost constant (or slightly increasing) area per lipid. The corresponding value of 0.75 nm^2 (averaged over the last 1 ns) is, however, significantly higher than the value of 0.64

TABLE 2 Lateral (D_{xy}) and transverse (D_z) diffusion coefficients for TRH and DPPC (lateral only) molecules during the different simulations

		TRH			DPPC
C_{TRH} (m)	T (K)	D_{xy} (10^{-5} cm^2 s^{-1})	D_z (10^{-5} cm^2 s^{-1})	ΔR_z^2 (nm^2)	D_{xy} (10^{-5} cm^2 s^{-1})
0	325	–	–	–	0.014
1	325	0.135	0.115	0.80	0.031
2	325	0.149	0.101	0.74	0.037
0	475	–	–	–	0.273
1	475	1.02	4.53	7.36	0.139
2	475	1.05	5.47	2.76	0.125

The plateau value (ΔR_z^2) of the mean-square displacement along the z axis is also reported for TRH.

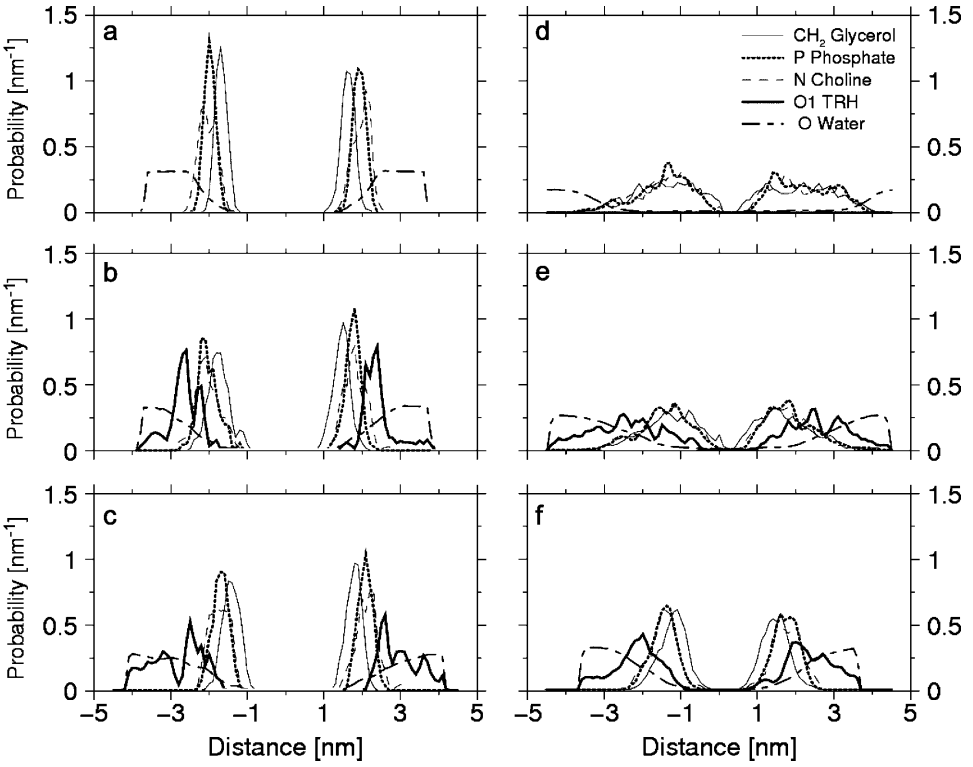

FIGURE 4 Normalized density profiles for specific atoms of DPPC, TRH, and water along the bilayer normal (z axis) calculated for the simulations without TRH (*a* and *d*), with TRH 1 m (*b* and *e*), or with TRH 2 m (*c* and *f*), at either 325 K (*left panels*) or 475 K (*right panels*). The profiles correspond to averages over the last 0.25 ns of each simulation.

nm^2 suggested as the best experimental estimate for a fully hydrated DPPC membrane in the liquid-crystalline phase at 325 K (Nagle and Tristram-Nagle, 2000). The time evolution of the box volume (Fig. 2 *d*) shows that, although the systems without TRH and with TRH 1 m undergo an important lateral contraction, the temperature increase nevertheless leads to an overall expansion of the system. This expansion is, however, almost negligible for the system with TRH 2 m. These results indicate that solely the latter simulation may describe a system at equilibrium.

The distributions of specific DPPC and water atoms along the bilayer normal, averaged over the last 0.25 ns of the simulation without TRH (Fig. 4 *d*), provide the explanation for the dramatic decrease in the area per lipid. In this simulation the bilayer structure is nearly entirely disrupted (compare with Fig. 4 *a* at 325 K). The distribution of the headgroups and glycerol atoms almost completely overlap and are largely broadened. The clear separation between the two layers is no longer observed, and the water distribution extends over the entire range of distances. The preservation of the membrane structure is slightly improved in the simulation containing TRH 1 m (Fig. 4 *e*). In contrast, upon inclusion of TRH 2 m, the integrity of the bilayer is maintained throughout the simulation (Fig. 4 *f*), a rather astonishing result considering the extreme temperature imposed to this system. Although the probability distributions for the lipid atoms are broader than at 325 K, the membrane can clearly be characterized as a bilayer. The distribution of the glycerol atoms is clearly distinguishable from that of the headgroup atoms, the latter oriented toward the aqueous phase. As was the case at 325 K, the distribution evidences a high affinity of TRH molecules for the bilayer surfaces but no significant desolvation of the lipid headgroups upon TRH coating (Fig. 4 *f*).

The different behavior of the bilayer during the high-temperature simulations is better appreciated by examining

TABLE 3 Average number of hydrogen bonds and probability of hydrogen bond formation between all species present in the simulations at 325 K

	TRH–DPPC		TRH–TRH		TRH–water		DPPC–water		
C_{TRH}	1 m	2 m	1 m	2 m	1 m	2 m	0 m	1 m	2 m
H-bonds	95.70	114.52	25.97	93.74	683.19	1373.00	552.06	449.48	435.52
SD	8.77	6.16	4.08	8.85	15.99	28.27	12.38	10.22	12.94
Probability (%)	1.168	0.699	0.652	0.567	0.320	0.321	0.118	0.105	0.102
SD (%)	0.141	0.046	0.163	0.053	0.007	0.007	0.003	0.002	0.003

Standard deviations (SD) are reported for the two quantities. The averages are calculated over the interval 2.0–6.0 ns for each simulation.

the configurations of the systems at the end of the three 6-ns simulations (Fig. 5). The thermally induced disruption of the membrane structure in the absence of TRH is evident in Fig. 5 *b*. At a concentration of 1 m, TRH is already able to reduce the disruptive effect of the temperature (Fig. 5 *c*). However, only at a 2-m TRH concentration can the membrane clearly be recognized as a bilayer (Fig. 5 *d*).

The analysis of the order parameters (S_{CD}) for the DPPC *sn*-1 and *sn*-2 chains at 475 K reveals a strong effect of the TRH concentration (Fig. 3, *c* and *d*). In the absence of TRH, the disorder of the chains is considerably enhanced compared to the results at 325 K and to the experimental data for the *sn*-2 chain, a consequence of the increased thermal motion and of the membrane disruption. This extent of disorder is, however, systematically reduced upon increasing the TRH concentration. The effect is more pronounced for the carbon atoms close to the headgroups. This might be due to a closer proximity with the TRH coating layer or a better residual alignment with the *z* axis. Although the simulation with TRH 2 m presents a stable bilayer structure, the corresponding order parameters remain significantly lower compared to the corresponding simulation at 325 K and to experiment. This is probably a consequence of both the elevated temperature and the concomitant increase in the area per lipid.

The lateral diffusion coefficients for water, TRH, and DPPC molecules (Tables 1 and 2) are from one to two orders of magnitude higher than the corresponding values at 325 K, a consequence of the increased thermal motion. Here also, only limited differences are observed between the simulations at different TRH concentrations. The only exception is a twofold decrease in the lateral diffusion coefficient of DPPC upon including TRH in the system. Interestingly, the lateral diffusion of TRH molecules at 475 K is about five times slower than their transverse diffusion, whereas it was 20–50% faster at 325 K. The relative reduction of the lateral mobility (compared to the transverse one) is probably a consequence of the TRH clustering and of its tighter interaction with the membrane surface at higher temperature (see below). Note also the abnormally high value of ΔR_z^2 for water in the simulation without TRH, which is due to the disruption of the membrane, allowing for larger displacements along the *z* axis (bilayer normal).

Since the inclusion of the disaccharide does not induce order-of-magnitude changes in the diffusional dynamics of the systems, it is unlikely that the preservation of the membrane structure in the presence of TRH 2 m is merely a kinetic effect (membrane disruption taking longer than the 6-ns simulation time). Rather, the membrane preservation appears to result from an increased thermodynamical stability.

The H-bond analysis during the simulations at 475 K (Table 4) reveals an overall decrease (32–46% for the different systems) in the total number of H-bonds compared to the simulations at 325 K (Table 3), as expected from the increased thermal motion. The decrease is also evident in the TRH–TRH, TRH–water, and DPPC-water components taken individually. For example, the number of DPPC–water H-bonds decreases by 37% and 41% for the systems with TRH 1 m and 2 m, respectively. Interestingly, however,

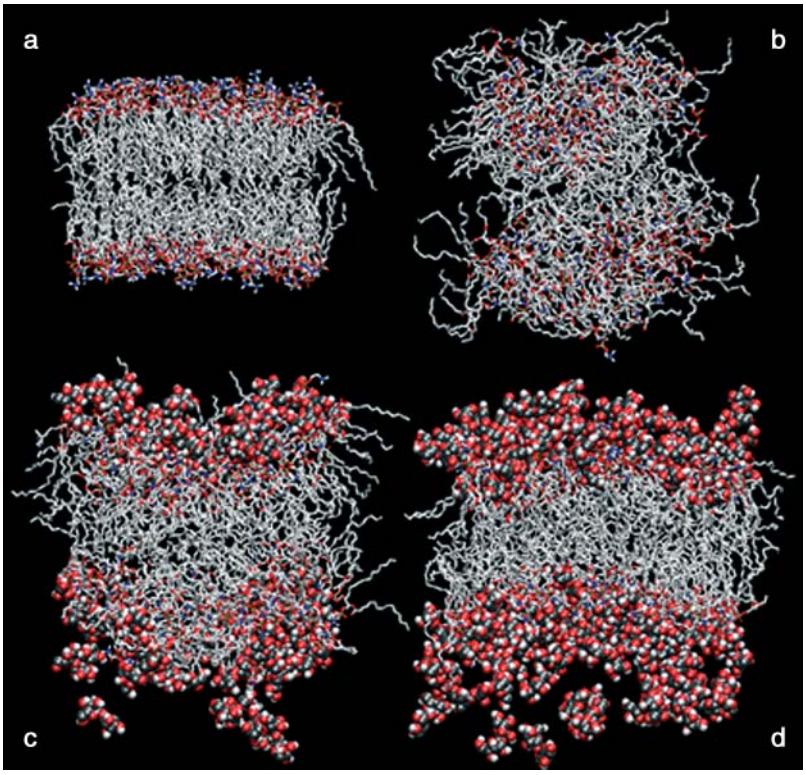

FIGURE 5 Final configurations of the systems without TRH at 325K (*a*), without TRH at 475 K (*b*), with TRH 1 m at 475 K (*c*), and with TRH 2 m at 475 K (*d*). DPPC molecules are represented using a stick model, TRH molecules using a space-fill model. Water molecules have been removed for clarity. Carbon atoms are represented in gray, oxygen atoms in red, phosphorous atoms in yellow, nitrogen atoms in blue, and hydrogen atoms in white.

TABLE 4 Average number of hydrogen bonds and probability of hydrogen bond formation between all the species present in the simulations at 475 K

	TRH–DPPC		TRH–TRH		TRH–water		DPPC–water		
C_{TRH}	1 m	2 m	1 m	2 m	1 m	2 m	0 m	1 m	2 m
H-bonds	116.77	190.27	17.27	58.15	432.65	859.91	295.21	285.38	255.88
SD	10.39	12.11	4.90	7.44	22.38	26.42	36.79	19.01	17.65
Probability (%)	1.425	1.161	0.409	0.359	0.202	0.201	0.063	0.067	0.060
SD (%)	0.157	0.137	0.102	0.047	0.010	0.006	0.008	0.004	0.004

Standard deviations (SD) are reported for the two quantities. The averages are calculated over the interval 2.0–6.0 ns for each simulation.

the number of TRH–DPPC H-bonds shows exactly the opposite trend, increasing by 22% and 67%, respectively, upon increasing the temperature. Accordingly, the fraction of the H-bonding sites provided by the membrane at which TRH replaces water (about one-fifth at 325 K) increases to 25% (TRH 1 m) or 43% (TRH 2 m). It could be argued that the above increase in the number of TRH–DPPC H-bonds is merely caused by a faster diffusion of TRH molecules toward the membrane surfaces at elevated temperature. However, this is probably not the case because 1), the TRH distribution was initially preequilibrated for 5 ns at 500 K, and 2), the diffusion of TRH is not dramatically (i.e., only about seven times) faster at 475 K compared to 325 K (Table 2). Therefore, the increase in the number of H-bonds appears to be thermodynamically driven. This finding also agrees with a recent infrared spectroscopic study of a binary lipid mixture in the absence and presence of TRH, showing that the direct interaction between lipid headgroups and TRH becomes stronger upon increasing the temperature (Ricker et al., 2003). Note, finally, that the saturation effect observed at 325 K for the TRH–DPPC H-bonds upon doubling the TRH concentration is significantly reduced at 475 K. The average number of TRH–DPPC H-bonds increases here by a factor of 1.6 upon doubling the TRH concentration, whereas at 325 K, this number increased by a factor 1.2.

The nature of the TRH–DPPC H-bonds is analyzed in more details in Table 5. TRH molecules are able to form multiple H-bonds simultaneously, sometimes with the same DPPC molecule and sometimes with distinct ones. Configurations where a single TRH molecule forms as many as eight H-bonds with lipid molecules have been observed in the simulations. Comparing the occurrences of the different H-bonding patterns at 325 K and 475 K, interesting observations can be made. At 325 K most of the TRH molecules (72% or 85% for TRH 1 m or 2 m respectively) belong to the patterns 0, 1, or 11, i.e., are either not hydrogen bonded to the bilayer or form a single H-bond with one or two distinct DPPC molecules. Upon increasing the temperature, the occurrences of these three patterns are reduced (to 62% or 69% for TRH 1 m or 2 m, respectively). In contrast, the occurrences of all other patterns, involving multiple H-bonds to the same DPPC molecule and/or the bridging of multiple DPPC molecules by a common TRH molecule, nearly systematically increase (the only exception being, patterns 21, 22, and 311 for TRH 1 m). Because the bridging of multiple DPPC molecules by a common TRH molecule seems to be a key factor for the membrane stabilization at high temperature, the occurrence of TRH molecules with a specific degree of bridging (i.e., forming at least one H-bond with a given number of distinct DPPC molecules) is analyzed in Table 6. The results clearly evidence that the dominant contribution to the increase in the number of TRH–DPPC H-bonds upon increasing the temperature is an increase in the degree of bridging of TRH molecules, i.e., an increased likelihood of finding TRH molecules H-bonded to three or more distinct DPPC molecules. The changes in the degree of bridging account for 63–65% of the increase in the total number of TRH–DPPC H-bonds. The remaining contribution is due to an increase in the average multiplicity of H-bonds between TRH and DPPC molecules.

TABLE 5 Average number of TRH molecules forming a specific H-bonding pattern with DPPC molecules during the simulations with TRH 1 m or 2 m at either 325 K or 475 K

Pattern	1 m, 325 K	1 m, 475 K	2 m, 325 K	2 m, 475 K
0	19.16	17.02	68.63	49.50
1	15.91	12.98	24.05	22.42
11	11.29	9.43	16.50	15.82
111	2.63	3.96	3.10	6.29
1111	0.30	1.11	0.58	1.32
11111	0.00	0.27	0.00	0.12
2	3.09	4.78	4.53	7.49
21	6.27	5.45	6.34	9.84
211	1.81	3.29	2.81	6.30
2111	0.46	1.24	0.56	2.09
22	0.59	0.43	0.27	0.75
221	0.42	0.45	0.15	0.88
3	0.50	0.65	0.17	1.12
31	0.61	0.67	0.21	1.25
311	0.62	0.53	0.05	0.92
32	0.01	0.04	0.01	0.08
4	0.01	0.07	0.00	0.18
41	0.03	0.05	0.00	0.16
5	–	0.00	–	0.01
Others	0.29	1.53	0.04	1.45
Total	64	64	128	128

A pattern is noted by series of integers (in descending order) indicating the number of H-bonds formed between a TRH molecule and a series of DPPC molecules. A zero indicates molecules forming no H-bonds to DPPC, whereas ''Others'' indicates TRH molecules forming more than five H-bonds. The averages are calculated over the interval 2.0–6.0 ns for each simulation.

TABLE 6 Average number of TRH molecules bridging a specific number of distinct DPPC molecules through (possibly multiple) H-bonds during the simulations with TRH 1 m or 2 m at either 325 K or 475 K

Degree of bridging	1 m, 325 K	1 m, 475 K	Contribution (%)	2 m, 325 K	2 m, 475 K	Contribution (%)
0	19.16	17.02	–	68.63	49.50	–
1	15.91	12.98	−14	24.05	22.42	−2
2	18.80	16.07	−26	23.33	27.91	12
3	5.50	8.35	41	6.11	14.55	33
4	0.96	2.89	37	1.17	4.23	16
5	0.07	0.84	18	0.01	0.54	4
Others	0.00	0.3	9	0.00	0.02	0.2
Total	64	64	65	128	128	63

A zero indicates molecules forming no H-bonds to DPPC, whereas ''Others'' indicates TRH molecules bonded to more than five distinct DPPC molecules. The relative contribution of each bridging pattern to the increase in the total number of TRH–DPPC H-bonds at 475 K is also indicated. The averages are calculated over the interval 2.0–6.0 ns for each simulation.

Comparison of the simulations at 325 and 475 K

The simulations at 325 K suggest that at this temperature, the presence of TRH does not significantly alter the membrane structure and dynamics. The TRH molecules clearly show a high affinity for the membrane surface and interact with DPPC molecules via H-bonds. However, water is not completely expelled from the bilayer surfaces by the clustering of TRH molecules. At the two concentrations considered, about one-fifth of the DPPC–water H-bonds occurring in the absence of TRH are actually replaced by H-bonds to the disaccharide. At this temperature, ~80% of the TRH molecules form either no H-bond to DPPC or a single H-bond to either one or two distinct DPPC molecules, but molecules forming more complex H-bonding patterns are also observed.

At 475 K, the membrane initially undergoes a significant lateral expansion. Afterwards, the behavior of the system depends crucially on the TRH concentration. In the absence of TRH, the membrane collapses into a structure that cannot be recognized as a bilayer. In the presence of TRH 1 m, the disruptive effect of the temperature is somewhat reduced. However, only in the system with TRH 2 m is the bilayer integrity maintained throughout the simulation. At this concentration, the protective action of TRH appears to be correlated with a significant increase (67%) in the number of TRH–DPPC H-bonds upon raising the temperature (although the total number of H-bonds in the system decreases by 32%). Furthermore, this increase can be dominantly attributed to a large increase in the number of TRH molecules bridging three or more lipid molecules through multiple H-bonds. This suggests that, after the initial thermal expansion of the membrane, TRH intercalates between the lipid headgroups and prevents the collapse of the membrane to an unstructured state by forming bridging H-bonds. TRH also significantly reduces the mobility of lipid chains, leading to both increased order parameters (this effect is also related with an enhanced alignment of the lipid chains in the bilayer normal direction) and reduced lateral diffusion of the DPPC molecules. The key role played by TRH–DPPC H-bonds in the stabilization of the membrane structure under unfavorable external conditions is in qualitative agreement with the results of several experimental studies (Crowe et al., 1984; Lee et al., 1986; Nakagaki et al., 1992; Tsvetkova et al., 1998; Nagase et al., 1999; Luzardo et al., 2000; Lambruschini et al., 2000; Ricker et al., 2003).

CONCLUSIONS

The aim of this study was to investigate the interaction of the disaccharide TRH with a DPPC bilayer at two different temperatures using MD simulations.

When interpreting the simulation results in terms of the three main hypotheses for the mechanism underlying the protective action of TRH (water replacement, water entrapment, or vitrification), it should be kept in mind that these simulations only probe a given type of biostructure (DPPC membrane) and environmental stress (artificially elevated temperature), a given concentration range (0–2 m TRH), and a rather short timescale (6 ns). On the other hand, the three above-mentioned hypotheses have been dominantly based on experimental data involving completely (or almost completely) dehydrated biostructures. Keeping these restrictions in mind, the results are most easily interpreted in the context of the water-replacement hypothesis, because 1), direct H-bonding interactions between DPPC and TRH molecules are observed, and 2), these interactions are enhanced when the membrane is subject to thermal stress. However, the term replacement may be misleading here, since water is not completely expelled from the membrane surface and only a fraction (about one-fifth at 325 K and up to twice as much at 475 K) of the DPPC–water H-bonds is substituted by DPPC–TRH H-bonds. Complete water replacement might occur in conditions of almost complete dehydration, which were not considered in this study. The vitrification hypothesis cannot be retained to account for the membrane stabilization at 475 K, because the diffusion constants for the different species in the system are only weakly affected by the TRH concentration. Thus, as expected, the system remains diffusive (as opposed to glassy) up to 2-m TRH concentration. Finally, these observa-

tions concerning a TRH-membrane system contrast with previous simulation results for TRH-protein systems at room temperature (Cottone et al., 2002; Lins et al., 2003). In these studies, TRH was found not to interact directly with the protein through H-bonds. Rather, coating by TRH preserved a thin layer of water molecules at the surface of the protein, providing support for the water-entrapment hypothesis. This apparent discrepancy suggests that the mechanism of stabilization by TRH may be nonspecific and vary depending on the nature of the biostructures involved and of the stress imposed to the system.

Note added in proof: During the processing of this article, another simulation study of a trehalose-membrane system has appeared in this journal (Sum et al., 2003. *Biophys. J.* 85:2830-2844). It is comforting to see that the conclusions reached by the two independent theoretical studies are in agreement with respect to most key observations.

The authors thank Mika Kastenholz and Chris Oostenbrink for valuable help with the analysis programs.

C.S.P. thanks the Coordenação de Aperfeiçoamento de Pessoal de Nivel Superior (CAPES) for support through a fellowship (BEX0480/02-9). Financial support by the Swiss National Foundation grant 21-63408 and the National Center of Competence in Research is gratefully acknowledged.

REFERENCES

Ballone, P., M. Marchi, C. Branca, and S. Magazu. 2000. Structural and vibrational properties of trehalose: a density functional study. *J. Phys. Chem. B.* 104:6313–6317.

Behm, C. A. 1997. The role of trehalose in the physiology of nematodes. *Int. J. Parasitol.* 27:215–229.

Belton, P. S., and A. H. Gil. 1994. IR and Raman spectroscopic studies of the interaction of trehalose with hen egg white lysozyme. *Biopolymers.* 34:957–961.

Berendsen, H. J. C., J. P. M. Postma, W. F. van Gunsteren, A. DiNola, and J. R. Haak. 1984. Molecular dynamics with coupling to an external bath. *J. Chem. Phys.* 81:3684–3690.

Berendsen, H. J. C., J. P. M. Postma, W. F. van Gunsteren, and J. Hermans. 1981. Interaction models for water in relation to protein hydration. *In* Intermolecular Forces. B. Pullman, editor. Reidel, Dordrecht, The Netherlands. 331–342.

Birch, G. G. 1972. Mushroom sugar. *In* Health and Food. G. G. Birch, L. F. Green, and I. G. Plaskett, editors. Elsevier Science, New York. 49–53.

Branca, C., S. Magazu, G. Maisano, S. M. Bennington, and B. Fak. 2003. Vibrational studies on disaccharide/H2O systems by inelastic neutron scattering, Raman, and IR spectroscopy. *J. Phys. Chem. B.* 107:1444–1451.

Branca, C., S. Magazu, G. Maisano, and P. Migliardo. 1999. Anomalous cryoprotective effectiveness of trehalose: Raman scattering evidences. *J. Chem. Phys.* 111:281–287.

Bryant, G., and J. Wolfe. 1992. Interfacial forces in cryobiology and anhydrobiology. *Cryo-Letters.* 13:23–36.

Carpenter, J. F., S. J. Prestrelski, T. J. Anchordoguy, and T. Arakawa. 1994. Interactions of stabilizers with proteins during freezing and drying. *In* Formulation and Delivery of Proteins and Peptides. J. L. Cleland and R. Langer, editors. American Chemical Society, Washington, DC. 134–147.

Chandrasekhar, I., and B. P. Gaber. 1988. Stabilization of the biomembrane by small molecules: interaction of trehalose with the phospholipids bilayer. *J. Biomol. Struct. Dyn.* 5:1163–1171.

Chandrasekhar, I., M. Kastenholz, R. D. Lins, C. Oostenbrink, L. D. Schuler, D. P. Tieleman, and W. F. van Gunsteren. 2003. A consistent potential energy parameter set for lipids: dipalmitoylphosphatidylcholine as a benchmark of the GROMOS96 45A3 force field. *Eur. Biophys. J.* 32:67–77.

Clegg, J. S. 1965. The origin of trehalose and its significance during formation of encysted dormant embryos of *Artemia salina*. *Comp. Biochem. Physiol.* 14:135–143.

Clegg, J. S. 1997. Embryos of *Artemia franciscana* survive four years of continuous anoxia: the case for complete metabolic rate depression. *J. Exp. Biol.* 200:467–475.

Clegg, J. S. 2001. Cryptobiosis—a peculiar state of biological organization. *Comp. Biochem. Physiol.* 128B:613–624.

Clegg, J. S., and S. A. Jackson. 1992. Aerobic heat-shock activates trehalose synthesis in embryos of *Artemia franciscana*. *FEBS Lett.* 303:45–47.

Conrad, P. B., and J. J. de Pablo. 1999. Computer simulation of the cryoprotectant disaccharide alpha, alpha-trehalose in aqueous solution. *J. Phys. Chem. A.* 103:4049–4055.

Cottone, G., G. Ciccotti, and L. Cordone. 2002. Protein-trehalose-water structures in trehalose coated carboxy-myoglobin. *J. Chem. Phys.* 117: 9862–9866.

Cottone, G., L. Cordone, and G. Ciccotti. 2001. Molecular dynamics simulation of carboxy-myoglobin embedded in a trehalose-water matrix. *Biophys. J.* 80:931–938.

Crowe, L. M. 2002. Lessons from nature: the role of sugars in anhydrobiosis. *Comp. Biochem. Physiol.* 131A:505–513.

Crowe, J. H., J. F. Carpenter, and L. M. Crowe. 1998a. The role of vitrification in anhydrobiosis. *Annu. Rev. Physiol.* 60:73–103.

Crowe, J. H., J. S. Clegg, and L. M. Crowe. 1998b. Anhydrobiosis: the water replacement hypothesis. *In* The Properties of Water in Foods (ISO-POW 6). D. S. Reid, editor. Chapman and Hall, New York. 440–455.

Crowe, J. H., L. M. Crowe, J. F. Carpenter, S. Prestrelski, F. A. Hoekstra, P. de Araújo, and A. D. Panek. 1997. Anhydrobiosis: cellular adaptation to extreme dehydration. *In* Handbook of Physiology, Vol. 2. W. H. Dantzler, editor. Oxford University Press, Oxford, UK. 1445–1477.

Crowe, J. H., L. M. Crowe, J. F. Carpenter, and C. A. Wistrom. 1987. Stabilization of dry phospholipid bilayers and proteins by sugars. *Biochem. J.* 242:1–10.

Crowe, J. H., L. M. Crowe, and D. Chapman. 1984. Preservation of membranes in anhydrobiotic organisms: the role of trehalose. *Science.* 223:701–703.

Crowe, J. H., L. M. Crowe, A. E. Oliver, N. Tsvetkova, W. Wolkers, and F. Tablin. 2001. The trehalose myth revisited: introduction to a symposium on stabilization of cells in the dry state. *Cryobiology.* 43:89–105.

Crowe, J. H., F. A. Hoekstra, and L. M. Crowe. 1992. Anhydrobiosis. *Annu. Rev. Physiol.* 54:579–599.

Crowe, J. H., A. E. Oliver, and F. Tablin. 2002. Is there a single biochemical adaptation to anhydrobiosis? *Integr. Comp. Biol.* 42:497–503.

Crowe, J. H., F. Tablin, W. F. Wolkers, K. Gousset, N. M. Tsvetkova, and J. Ricker. 2003. Stabilization of membranes in human platelets freeze-dried with trehalose. *Chem. Phys. Lipids.* 122:41–52.

Damore, T. G., R. G. Crumplen, and G. G. Stewart. 1991. The involvement of trehalose in yeast stress tolerance. *J. Ind. Microbiol.* 7:191–195.

Douliez, J. P., A. Leonard, and E. J. Dufourc. 1995. Restatement of order parameters in biomembranes: calculation of C–C bond order parameters from C-D quadrupolar splittings. *Biophys. J.* 68:1727–1739.

Egberts, E., and H. J. C. Berendsen. 1988. Molecular dynamics simulation of a smectic liquid crystal with atomic detail. *J. Chem. Phys.* 89:3718–3732.

Ekdawi-Sever, N., J. J. de Pablo, E. Feick, and E. von Meerwall. 2003. Diffusion of sucrose and alpha, alpha-trehalose in aqueous solutions. *J. Phys. Chem. A.* 107:936–943.

Elbein, A. D., Y. T. Pan, I. Pastuszak, and D. Carrol. 2003. New insights on trehalose: a multifunctional molecule. *Glycobiology*. 13:17R–27R.

Eleutherio, E. C. A., J. T. Silva, and A. Panek. 1993. Role of the trehalose carrier in dehydration resistance of *S. cervisiae*. *Biochim. Biophys. Acta*. 1156:263–266.

Engelsen, S. B., and S. Perez. 2000. Unique similarity of the asymmetric trehalose solid-state hydration and the diluted aqueous-solution hydration. *J. Phys. Chem. B*. 104:9301–9311.

Eroglu, A., M. Toner, and T. L. Toth. 2002. Beneficial effect of microinjected trehalose on the cryosurvival of human oocytes. *Fertil. Steril*. 77:152–158.

Feofilova, E. P. 2003. Deceleration of vital activity as a universal biochemical mechanism ensuring adaptation of microorganisms to stress factors: a review. *Appl. Biochem. Microbiol*. 39:1–18.

Fukuse, T., T. Hirata, T. Nakamura, M. Ueda, M. Kawashima, S. Hitomi, and H. Wada. 1999. Role of saccharides on lung preservation. *Transplantation*. 68:110–117.

Guppy, M., and P. Withers. 1999. Metabolic depression in animals: physiological perspectives and biochemical generalizations. *Biol. Rev*. 74:1–40.

Hockney, R. W. 1970. The potential calculation and some applications. *Methods Comput. Phys*. 9:136–211.

Hoekstra, F. A., W. F. Wolkers, J. Buitink, E. A. Golovina, J. H. Crowe, and L. M. Crowe. 1997. Membrane stabilization in the dry state. *Comp. Biochem. Physiol*. 117A:335–341.

Keilin, D. 1959. The problem of anabiosis or latent life: history and current concept. *Proc. R. Soc. Lond. B Biol. Sci*. 150:149–191.

Koch, E. M., and F. C. Koch. 1925. The presence of trehalose in yeast. *Science*. 61:570–572.

Koster, K. L., Y. P. Lei, M. Anderson, S. Martin, and G. Bryant. 2000. Effects of vitrified and nonvitrified sugars on phosphatidylcholine fluid-to-gel phase transitions. *Biophys. J*. 78:1932–1946.

Koster, K. L., M. S. Webb, and G. Bryant. 1994. Interactions between soluble sugars and POPC (1-palmitoyl-2-oleoylphosphatidylcholine) during dehydration: vitrification of sugars alters the phase-behavior of the phospholipid. *Biochim. Biophys. Acta*. 1193:143–150.

Lambruschini, C., N. Relini, A. Ridi, L. Cordone, and A. Gliozzi. 2000. Trehalose interacts with phospholipid polar heads in Langmuir monolayers. *Langmuir*. 16:5467–5470.

Lee, C. W. B., J. S. Waugh, and R. G. Griffin. 1986. Solid-state NMR-study of trehalose/1,2-dipalmitoyl-sn-phosphatidylcholine interactions. *Biochemistry*. 25:3737–3742.

Lins, R. D., C. S. Pereira, and P. H. Hünenberger. 2004. Trehalose-protein interaction in aqueous solution. *Proteins*. 55:177–186.

Liu, Q., R. K. Schmidt, B. Teo, P. A. Karplus, and J. W. Brady. 1997. Molecular dynamics studies of the hydration of alpha, alpha-trehalose. *J. Am. Chem. Soc*. 119:7851–7862.

Luzardo, M. D., F. Amalfa, A. M. Nunez, S. Diaz, A. C. B. de Lopez, and E. A. Disalvo. 2000. Effect of trehalose and sucrose on the hydration and dipole potential of lipid bilayers. *Biophys. J*. 78:2452–2458.

Madin, K. A. C., and J. Crowe. 1975. Anhydrobiosis in nematodes: carbohydrate and lipid metabolism during drying. *J. Exp. Zool*. 193:335–342.

Matsuo, T. 2001. Trehalose protects corneal epithelial cells from death by drying. *Br. J. Ophthalmol*. 85:610–612.

Matsuo, T., Y. Tsuchida, and N. Morimoto. 2002. Trehalose eye drops in the treatment of dry eye syndrome. *Ophthalmology*. 109:2024–2029.

Nagase, H., H. Ueda, and M. Nakagaki. 1999. Relationship between hydrophobic index of saccharide and gel-liquid crystal transition temperature of the L-alpha-dipalmitoyl phosphatidylcholine (DPPC)/saccharide/water system. *Chem. Pharm. Bull*. 47:607–610.

Nagle, J. F., and S. Tristram-Nagle. 2000. Structure of lipid bilayers. *Biochim. Biophys. Acta*. 1469:159–195.

Nakagaki, M., H. Nagase, and H. Ueda. 1992. Stabilization of the lamellar structure of phosphatidylcholine by complex-formation with trehalose. *J. Membr. Sci*. 73:173–180.

Norcia, M. A. 2000. Compositions and methods for wound management. *Off. Gaz. Pat. Office*. 1232:424–448.

Oliver, A. E., O. Leprince, W. F. Wolkers, D. K. Hincha, A. G. Heyer, and J. H. Crowe. 2001. Non-disaccharide-based mechanisms of protection during drying. *Cryobiology*. 43:151–167.

Richards, A. B., S. Krakowka, L. B. Dexter, H. Schmid, A. P. M. Wolterbeek, D. H. Waalkens-Berendsen, A. Shigoyuki, and M. Kurimoto. 2002. Trehalose: a review of properties, history of use and human tolerance, and results of multiple safety studies. *Food Chem. Toxicol*. 40:871–898.

Ricker, J. V., N. M. Tsvetkova, W. F. Wolkers, C. Leidy, F. Tablin, M. Longo, and J. H. Crowe. 2003. Trehalose maintains phase separation in an air-dried binary lipid mixture. *Biophys. J*. 84:3045–3051.

Rudolph, B. R., I. Chandrasekhar, B. P. Gaber, and M. Nagumo. 1990. Molecular modeling of saccharide-lipid Interactions. *Chem. Phys. Lipids*. 53:243–261.

Ryckaert, J. P., G. Ciccotti, and H. J. C. Berendsen. 1977. Numerical integration of cartesian equations of motion of a system with constraints molecular dynamics of n-alkanes. *J. Comput. Phys*. 23:327–341.

Sackmann, E. 1995. Physical basis of self-organization and function of membranes: physics of vesicles. *In* Handbook of Biological Physics, Vol. 1A, Structure and Dynamics of Membranes. R. Lipowsky and E. Sackman, editors. Elsevier, Amsterdam, The Netherlands. 213–304.

Schuler, L. D., X. Daura, and W. F. van Gunsteren. 2001. An improved GROMOS96 force field for aliphatic hydrocarbons in the condensed phase. *J. Comput. Chem*. 22:1205–1218.

Scott, P. 2000. Resurrection plants and the secrets of the leaf. *Ann. Bot*. 85:159–166.

Singer, M. A., and S. Lindquist. 1998. Thermotolerance in Saccharomyces cerevisiae: the yin and yang of trehalose. *Trends Biotechnol*. 16:460–468.

Somme, L. 1996. Anhydrobiosis and cold tolerance in tardigrades. *Eur. J. Entomol*. 93:349–357.

Sun, W. Q., T. C. Irving, and A. C. Leopold. 1994. The role of sugar, vitrification and membrane phase-transition in seed desiccation tolerance. *Physiol. Plantarum*. 90:621–628.

Sun, W. Q., and A. C. Leopold. 1994. Glassy state and seed storage stability: a viability equation analysis. *Ann. Bot*. 74:601–604.

Sun, W. Q., and A. C. Leopold. 1997. Cytoplasmic vitrification acid survival of anhydrobiotic organisms. *Comp. Biochem. Physiol*. 117A: 327–333.

Sun, W. Q., A. C. Leopold, L. M. Crowe, and J. H. Crowe. 1996. Stability of dry liposomes in sugar glasses. *Biophys. J*. 70:1769–1776.

Sussich, F., C. Skopec, J. Brady, and A. Cesaro. 2001. Reversible dehydration of trehalose and anhydrobiosis: from solution state to an exotic crystal? *Carbohydr. Res*. 334:165–176.

Takahashi, H., H. Ohmae, and I. Hatta. 1997. Trehalose-induced destabilization of interdigitated gel phase in dihexadecylphosphatidylcholine. *Biophys. J*. 73:3030–3038.

Timasheff, S. N. 1982. The control of protein stability and association by weak-interactions with water. *In* Biophysics of Water. F. Franks and S. Mathias, editors. Wiley, New York. 70–72.

Tironi, I. G., R. Sperb, P. E. Smith, and W. F. van Gunsteren. 1995. A generalized reaction field method for molecular dynamics simulations. *J. Chem. Phys*. 102:5451–5459.

Tsvetkova, N. M., B. L. Phillips, L. M. Crowe, J. H. Crowe, and S. H. Risbud. 1998. Effect of sugars on headgroup mobility in freeze-dried dipalmitoylphosphatidylcholine bilayers: solid-state P-31 NMR and FTIR studies. *Biophys. J*. 75:2947–2955.

van Gunsteren, W. F., and H. J. C. Berendsen. 1990. Computer simulation of molecular dynamics: methodology, applications and perspectives in chemistry. *Angew. Chem. Int. Ed. Engl*. 29:992–1023.

van Gunsteren, W. F., S. R. Billeter, A. A. Eising, P. H. Hünenberger, P. Krüger, A. E. Mark, W. R. P. Scott, and I. G. Tironi. 1996. Biomolecular Simulation: The GROMOS96 Manual and User Guide. Hochschulverlag an der ETH Zürich/Biomos, Zürich/Groningen.

Westh, P., and H. Ramlov. 1991. Trehalose accumulation in the tardigrade adorybiotus-coronifer during anhydrobiosis. *J. Exp. Zool.* 258:303–311.

Williams, R. J., and A. C. Leopold. 1989. The glassy state in corn embryos. *Plant Physiol.* 89:977–981.

Wingler, A. 2002. The function of trehalose biosynthesis in plants. *Phytochemistry.* 60:437–440.

Wolfe, J., and G. Bryant. 1999. Freezing, drying and or vitrification of membrane-solute-water systems. *Cryobiology.* 39:103–129.

Wyatt, G. R., and G. F. Kalf. 1957. The chemistry of isect hemolymph. 2. Trehalose and other carbohydrates. *J. Gen. Physiol.* 40:833–847.

Xie, G. F., and S. N. Timasheff. 1997. The thermodynamic mechanism of protein stabilization by trehalose. *Biophys. Chem.* 64:25–43.

Zhang, J., and P. L. Steponkus. 1996. Proposed mechanism for depression of the liquid-crystalline-to-gel phase transition temperature of phospholipids in dehydrated sugar-phospholipid mixtures. *Cryobiology.* 33: 625–626.